Saturn's quasiperiodic magnetohydrodynamic waves

J. N. Yates[1], D. J. Southwood[1], M. K. Dougherty[1], A. H. Sulaiman[2], A. Masters[1], S. W. H. Cowley[3], M. G. Kivelson[4,5], C. H. K. Chen[1], G. Provan[3], D. G. Mitchell[6], G. B. Hospodarsky[2], N. Achilleos[7,8], A. M. Sorba[7,8], and A. J. Coates[8,9]

[1] Space and Atmospheric Physics, Imperial College London, London, UK, [2] Department of Physics and Astronomy, University of Iowa, Iowa City, Iowa, USA, [3] Department of Physics and Astronomy, University of Leicester, Leicester, UK, [4] Department of Earth, Planetary, and Space Sciences, University of California, Los Angeles, California, USA, [5] Climate and Space Sciences and Engineering, University of Michigan, Ann Arbor, Michigan, USA, [6] Johns Hopkins University Applied Physics Laboratory, Laurel, Maryland, USA, [7] Department of Physics and Astronomy, University College London, London, UK, [8] Centre for Planetary Sciences at UCL/Birkbeck, London, UK, [9] Mullard Space Science Laboratory, University College London, Surrey, UK

Abstract Quasiperiodic ∼1 h fluctuations have been recently reported by numerous instruments on board the Cassini spacecraft. The interpretation of the sources of these fluctuations has remained elusive to date. Here we provide an explanation for the origin of these fluctuations using magnetometer observations. We find that magnetic field fluctuations at high northern latitudes are Alfvénic, with small amplitudes (∼0.4 nT), and are concentrated in wave packets similar to those observed in Kleindienst et al. (2009). The wave packets recur periodically at the northern magnetic oscillation period. We use a magnetospheric box model to provide an interpretation of the wave periods. Our model results suggest that the observed magnetic fluctuations are second harmonic Alfvén waves standing between the northern and southern ionospheres in Saturn's outer magnetosphere.

1. Introduction

The Cassini spacecraft has been orbiting Saturn since 2004 where it has taken many observations using remote sensing and in situ instruments. A number of recent studies have reported ∼1 h quasiperiodic phenomena such as energetic ion conics, field-aligned energetic electron beams, auroral hiss, pulsating aurora, and magnetic field fluctuations at Saturn [*Mitchell et al.*, 2009, 2016; *Radioti et al.*, 2011, 2013; *Badman et al.*, 2012, 2016; *Meredith et al.*, 2013; *Bunce et al.*, 2014; *Roussos et al.*, 2016; *Palmaerts et al.*, 2016; *Carbary et al.*, 2016]. These studies used observations from the Radio and Plasma Wave Science (RPWS) [*Gurnett et al.*, 2004], Cassini Plasma Spectrometer (CAPS) [*Young et al.*, 2004], Magnetospheric Imaging Instrument (MIMI) [*Krimigis et al.*, 2004], Visual and Infrared Mapping Spectrometer (VIMS) [*Brown et al.*, 2004], and magnetometer (MAG) [*Dougherty et al.*, 2004] instruments on board the Cassini spacecraft. Such quasiperiodic phenomena is referred to as QP60 (quasiperiodic 60 m) fluctuations, but the origin of this relatively fixed period still remains an open question. Knowing the physical cause of such events could provide a "diagnostic" capable of inferring the dynamical conditions within Saturn's magnetosphere. In this study we use Cassini magnetic field observations and theoretical modeling to propose the source of this periodicity.

Mitchell et al. [2009] found field-aligned ion conics (of ionospheric source) and electron beams pulsing at ∼1 h intervals. Their events were seen predominantly in the evening local time (LT) sector and on magnetic shells beyond $L = 10 R_S$ (Saturn radii, 1 $R_S = 60,268$ km) and were usually accompanied by whistler mode waves and field-aligned current structures. *Mitchell et al.* [2009] concluded that these events resembled, in origin, terrestrial observations of downward field-aligned current regions [e.g., *Carlson et al.*, 1998]. *Badman et al.* [2012] also observed QP60 ion beams of ionospheric origin, electron beams, and whistler mode bursts coincident with downward current regions. However, these measurements were made around noon LT, in between upward field-aligned currents mapping to intense auroral arcs seen using the VIMS instrument. The events were attributed to transient reconnection events occurring on the dayside magnetopause. More recently, *Roussos et al.* [2016] and *Palmaerts et al.* [2016] carried out extensive studies on QP60 injections of energetic electrons using the MIMI-Low Energy Magnetospheric Measurement System (LEMMS) instrument. They showed that these injections are common throughout Saturn's magnetosphere but are generally found beyond Titan's orbit (∼20 R_S) and show a LT asymmetry with events being more common near dusk than near dawn.

Roussos et al. [2016] also showed that the injections map to magnetic flux tubes with foot points correlating well to regions of auroral emissions. In addition, *Palmaerts et al.* [2016] found that these events were sometimes coincident with whistler mode pulses and magnetic field fluctuations and proposed that such events could be initiated in a high-latitude acceleration region. All of the above fluctuating phenomena have periods of order ∼60 m.

Pulsations observed at Earth are typically associated with magnetohydrodynamic (MHD) waves [*Dungey*, 1955; *Takahashi et al.*, 2006; *Keiling*, 2009]. MHD waves are considered ultralow frequency (ULF) waves if their frequencies lie between ∼1 mHz and 1 Hz corresponding to periods ranging between 1 s and ∼17 m. These periods are much smaller than Earth's rotation rate, so plasma conditions in the terrestrial magnetosphere can be treated as stationary on ULF MHD wave timescales [*Glassmeier et al.*, 2004]. Terrestrial MHD waves have numerous sources and can lead to eigenoscillations of the entire magnetosphere [e.g., *Kivelson and Southwood*, 1985]. Much of the magnetosphere can be treated as cold to a first approximation, and in this regime there are two types of MHD waves: (i) the fast (compressional) wave and (ii) the shear Alfvén (noncompressional) wave. When the expected wavelengths are comparable to the scale of the magnetosphere, the compressional eigenmodes give rise to global wave structures. In nonuniform plasmas, the purely transverse Alfvén mode can only occur localized to particular magnetic shells. However, the two wave modes can resonantly couple to set up magnetic field line resonances (FLRs) [*Southwood*, 1974; *Chen and Hasegawa*, 1974] on the shells where the Alfvén mode dispersion relation is satisfied.

The allowed periods of FLRs can often be estimated using the time-of-flight method [*Warner and Orr*, 1979] giving the travel time for an Alfvén wave on a magnetic field line. In the outer solar system, *Glassmeier et al.* [1989] determined Alfvén travel times at Jupiter and Saturn to be comparable to their rotation rates, thus inhibiting the formation of global oscillations and FLRs. Nevertheless, ULF waves have been observed at Jupiter and Saturn [e.g., *Khurana and Kivelson*, 1989; *Cramm et al.*, 1998; *Kleindienst et al.*, 2009] but they are thought to be local waves, formed in specific regions/cavities within the magnetosphere and not global waves as for the Earth. Additionally, work by *Southwood and Kivelson* [1986] and *Khurana and Kivelson* [1989] suggests that the magnetic perturbations of Alfvén waves in gas giant magnetospheres are likely to reach maximum amplitude near the equator. More recent estimates applicable to Jupiter's and Saturn's outer magnetosphere suggest Alfvén travel times much smaller (∼10%) than the planetary rotation rate [*Bagenal et al.*, 2014; *Bunce et al.*, 2005] potentially allowing global MHD waves. A recent review on ULF phenomena at Saturn and Jupiter can be found in *Delamere* [2016].

Kleindienst et al. [2009] were the first to study ULF waves at Saturn using data from the Cassini spacecraft. They found wave activity throughout all regions sampled between July 2004 and March 2007. In addition, the ULF waves were typically nonsinusoidal, observed in wave packets, and had transverse amplitudes ≤0.5 nT. The waves were determined to be Alfvénic, and their occurrence correlated well with the 10.7 h oscillations in the background magnetic field. As such, they postulated that the waves may be modulated by the planetary rotation rate. *Kleindienst et al.* [2009] developed a time-varying rotation rate (similar to that derived in *Kurth et al.* [2007] based on oscillations of the southward background magnetic field component. Despite organizing the magnetic oscillations well, this rotation rate did not organize the observed wave packets. *Kleindienst et al.* [2009] nevertheless proposed that the ∼1 h magnetic fluctuations resulted from the decay of large-amplitude and long-period magnetic disturbances caused by a corotating magnetic field anomaly such as those proposed by *Southwood and Kivelson* [2007] and *Andrews et al.* [2010]. Saturn's radio rotation rate has been known to be time variable since the analysis of *Galopeau and Lecacheux* [2000], and we now also know that there are two radio rotation rates each separately observed in the northern or southern magnetosphere [*Gurnett et al.*, 2009]. The magnetic oscillation rotation rates closely match the radio rotation rates [*Andrews et al.*, 2012]. The magnetic rotation rates are, however, further complicated by the fact that both northern and southern oscillations are seen at equatorial latitudes, while only one pure (to within ∼10%) oscillation is observed at high latitudes [*Andrews et al.*, 2012; *Provan et al.*, 2012].

Meredith et al. [2013] investigated Hubble Space Telescope observations of small conjugate auroral patches at Saturn. The majority of the patches were located between dawn and noon local time and separated by 0.5–1 h LT. Employing a magnetospheric box model, they suggested that such auroral patches are caused by field-aligned currents of eastward propagating second harmonic Alfvén waves possibly generated by drift-bounce resonances of hot magnetospheric water ions. *Meredith et al.* [2013] determined the oscillation periods of their proposed Alfvén waves to be ∼40 m in the inertial frame and ∼80 m in the plasma rest frame,

which is of order ∼60 m fluctuations discussed. More recently, *Carbary et al.* [2016] used radio observations to statistically study QP60 whistler mode pulsations (at 100 Hz). They found that these events are more likely to be present at high latitudes and at evening sector local times. They proposed that interhemispheric Alfvén waves of similar transit times (calculated using the *Achilleos et al.* [2010] magnetic field model) should be considered as principal candidates for their production.

Using data from the Cassini magnetometer (MAG), we focus on the fluctuations of the magnetic field over a 6 day interval in 2006 and suggest a possible explanation for the recurrent ∼1 h period and the underlying nature of these fluctuations. We propose that this period likely results from an internal characteristic of the Kronian system and possibly associated with the travel of Alfvén mode waves. Our study is laid out as follows. In section 2 we present examples of the ULF magnetic fluctuations. Sections 3 and 4 present our results and discuss the possible sources of these magnetic fluctuations. We conclude in section 5.

2. Observations

Figures 1a and 1b show the Cassini spacecraft's trajectory during December 2006 in the Kronocentric Solar Magnetic (KSMAG) coordinate system (gray), which is centered on Saturn with the *Z* axis pointing along the magnetic dipole axis and the *Y* axis is the right-handed cross product between the *Z* axis and the direction of the Sun. The *X* axis lies in the plane created by the *Z* axis and sun direction and completes the right-handed orthogonal set [*Arridge et al.*, 2008]. Figure 1a shows the trajectories projected on the *X-Y* plane, while Figure 1b shows the same trajectories but for the *X-Z* plane. The blue lines indicate the data interval used in this study, and the blue crosses indicate day boundaries. The red cross indicates the start of the interval used here. A model magnetopause boundary obtained using a solar wind dynamic pressure of 0.02 nPa giving a typical subsolar magnetopause standoff distance of ∼22 R_S is also shown in black [*Kanani et al.*, 2010]. Throughout this interval Cassini was located at radial distances of ∼13–28 R_S away from Saturn, at ∼50–20° planetary latitude, and between ∼20:00 and 01:00 h LT. The spacecraft's location corresponds to dipole *L* shells between ∼ 30 and 40 R_S and invariant magnetic latitudes of ∼81°.

High northern latitude, 1 min resolution data from the Fluxgate Magnetometer instrument (MAG) [*Dougherty et al.*, 2004] on board the Cassini spacecraft are used in this study. Figure 1c shows a full orbit of magnetic field observations taken in December 2006. The field measurements are shown in the Kronocentric radial, theta, phi (KRTP) coordinate system, where the radial (*r*) axis points radially outward from the planet, the *θ* axis points in the direction of increasing colatitude, and the *ϕ* axis is in the local direction of planetary rotation. The blue, red, and green lines indicate the *r*, *θ*, and *ϕ* components of the magnetic field, respectively, while the black lines indicate ±|*B*|. Figure 1d shows a zoomed-in, 6 day portion of the residual magnetic field. The residual field is the difference between the measured field (in Figure 1c) and the internal magnetic field model of *Dougherty et al.* [2005], i.e., $d\mathbf{B} = \mathbf{B} - \mathbf{B_{int}}$. The colors follow the same scheme as in Figure 1c. Field-aligned currents (FACs) responsible for Saturn's main aurora are encountered approximately on day of year 337.5 and 348.7. These FACs are associated with the subcorotation of Enceladus plasma relative to Saturn's thermospheric neutrals and to the two current systems responsible for the global magnetic oscillations [*Hunt et al.*, 2014]. Poleward of these FACs, the field measurements exhibit the ∼10.7 h magnetic oscillations ubiquitously present within Saturn's magnetosphere [e.g., *Andrews et al.*, 2012]. These oscillations are clearly seen in (Figure 1d) and are the focus of this study. Figure 1e shows the electron density derived from the Langmuir probe (LP) on board the Cassini spacecraft. First, we note that these electron densities are all very low compared to those in the conjugate equatorial magnetodisc (order ∼1 cm^{-3}); in fact, they are comparable to the lobe densities presented in *Gurnett et al.* [2010]. The large, order-of-magnitude density variations appear quasi-sinusoidal on the logarithmic scale used indicating that a large electron density gradient is being swept back and forth across the spacecraft with a period of ∼10.7 h. This is likely caused by the observed rocking of the magnetosphere and/or motion from the flapping magnetotail at the magnetic oscillation periods.

Figures 1f–1h show parallel ($\delta b_{||}$) and perpendicular ($\delta b_{\perp \nu}$ and $\delta b_{\perp \phi}$) mean field-aligned (MFA) magnetic components respectively for this 6 day interval. $\delta b_{\perp \nu}$ lies in the meridional plane, while $\delta b_{\perp \phi}$ is essentially azimuthal. The MFA components were obtained by first subtracting a mean background field from the residual magnetic components. The mean background field was calculated using a 60 min moving average of the residual magnetic field. These were then transformed into MFA components in a similar fashion to that described in *Kleindienst et al.* [2009]. The results presented below are unaffected by time-averaging window
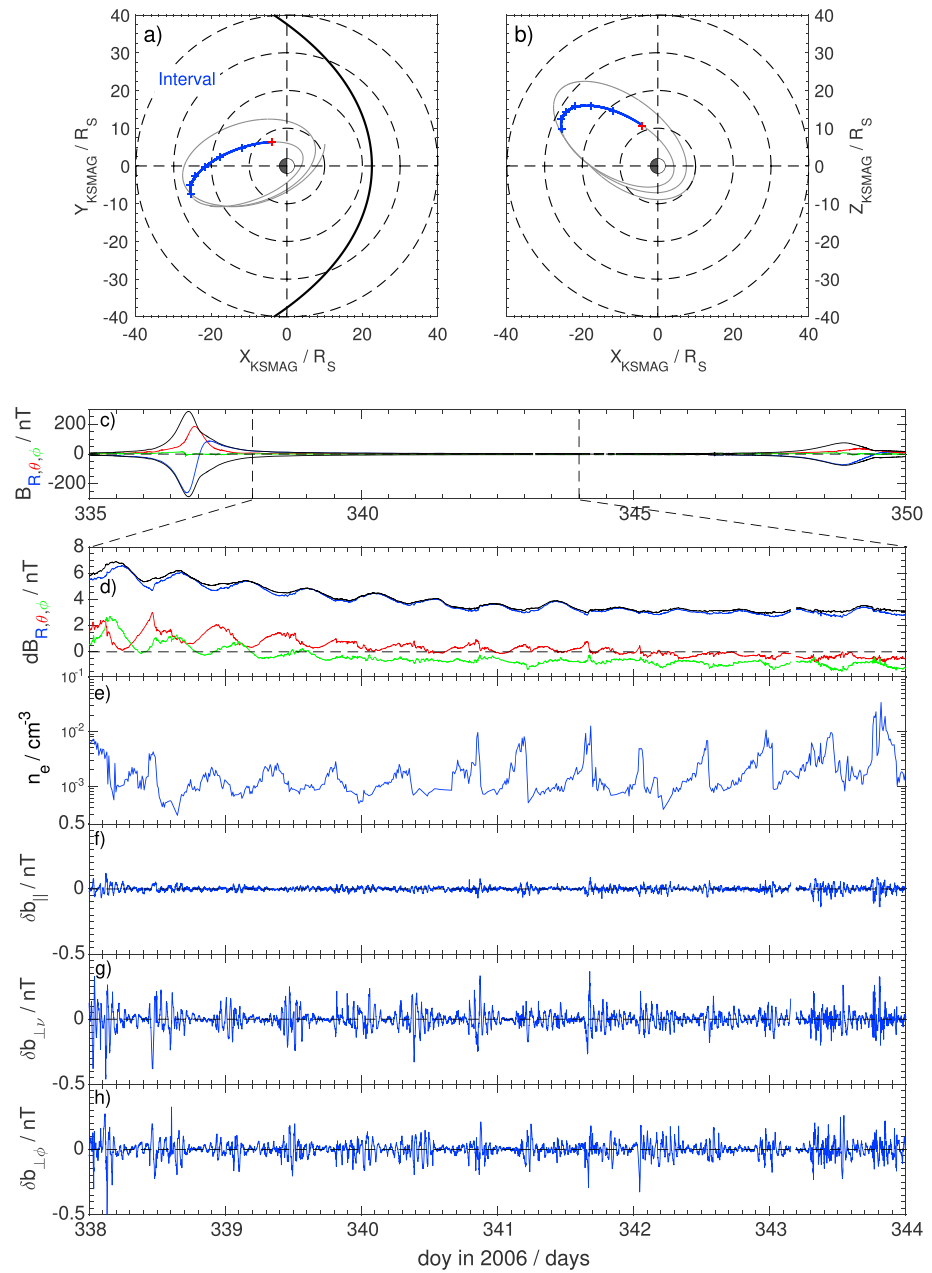
Figure 1. (a) Cassini's trajectory in the KSMAG *X-Y* plane (gray lines). The blue line indicates the interval used in this study where the start of each day is denoted by a blue cross. The start of our interval is indicated by the red cross. Saturn is in the center of the plot. The dashed black circles represent radii increasing in intervals of 10 R_S. A model magnetopause boundary (black line) is shown, based on the work of *Kanani et al.* [2010] (obtained using a solar wind dynamic pressure of 0.02 nPa giving a typical subsolar magnetopause standoff distance of ~22 R_S). (b) The same trajectory but in the KSMAG *X-Z* plane. (c) The KRTP magnetic field components as a function of time for one spacecraft orbit where radial, theta, and phi components are represented by the blue, red, and green lines, respectively. The black lines represent positive and negative magnitude of the magnetic field. (d) The residual magnetic field components within our analysis interval (4–10 December 2006) using the same color scheme as in Figure 1c. (e) Electron densities measured by the Langmuir Probe onboard Cassini. (f) The mean field-aligned component parallel to the background magnetic field. (g, h) The two transverse mean field-aligned components.
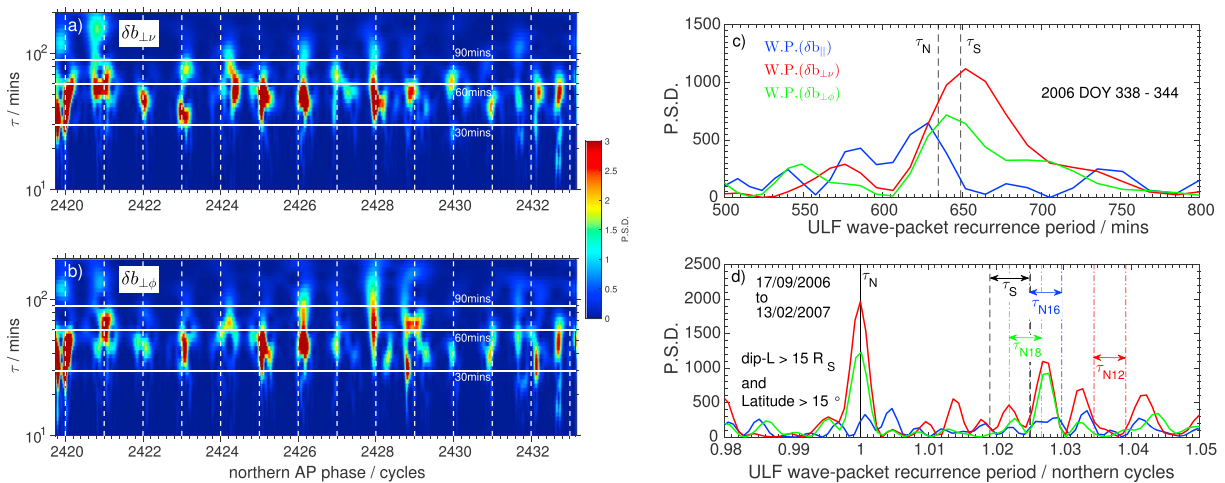
Figure 2. (a) The normalized wavelet power for $\delta b_{\perp\nu}$ in northern phase and inverse frequency (period) space. The horizontal, solid white lines indicate periods of 30, 60, and 90 min. The white vertical dashed lines indicate integer multiples of northern AP phase. (b) The same as Figure 2a but for $\delta b_{\perp\phi}$. (c) The Lomb-Scargle (LS) power spectral density (P.S.D.) corresponding to the maximum wavelet power (W.P.) as a function of the wave packet recurrence period in minutes for $\delta b_{\parallel}$ (blue), $\delta b_{\perp\nu}$ (red), and $\delta b_{\perp\phi}$ (green). The averaged northern and southern magnetic periods are indicated by the black dashed lines and are labeled accordingly. (d) LS PSDs as a function of northern AP phase (in cycles) for the northern portion of the inclined orbits in 2006 and 2007. We define the northern portions by selecting magnetometer data where the spacecraft latitude was >15° and the dipole L shell was >15 R_S. The northern cycle is indicated by the black solid line, while the range of the southern oscillation as seen in the northern reference frame is enclosed within the two black dashed lines. We also include ranges of the beat period between the northern magnetic oscillation and the repetitive spacecraft orbits of 12, 16, and 18 days in this interval. The repetitive nature of these orbits means that we obtain periodic data gaps which adds power to the LS analysis.

lengths between 30 and 180 m. Figures 1f–1h indicate the presence of wave packets, most evident in the perpendicular MFA components. The perpendicular wave packet amplitudes are modulated between ~0.1 nT and ~0.4 nT (with $\delta b/B \sim 0.02-0.1$), while the parallel wave packets are small and barely evident. The dominantly transverse nature of these wave packets suggests that they are Alfvénic. The fluctuations within each wave packet appear to have a period of order 60 min. Coincident ~60 m pulsed events, similar to those presented in previous studies, are also observed in the RPWS and, to a lesser extent, MIMI-LEMMS data sets shown in supporting information Figure S1.

3. QP Magnetic Fluctuation Period and Recurrence Rate

We begin by identifying the frequencies of the QP fluctuations within each wave packet in Figures 1f–1h. Following on from *Kleindienst et al.*'s [2009] hypothesis of a rotational dependence of the wave activity, we investigate the recurrence of the presented wave packets with relation to the northern and southern ~10.7 h magnetic oscillation phases as determined by *Andrews et al.* [2012]. These phases can be considered as a way of counting time where 360° of phase (or one cycle) represents one full rotation of either the northern or southern magnetic oscillation systems.

In order to determine the fluctuation frequencies present in each wave packet, we apply a continuous wavelet transform (CWT) to the MFA magnetic field components. Standard Fourier techniques are not used as signals containing wave packets are generally nonstationary, and a wavelet transform is capable of isolating individual, time-limited wave packets and determining what frequencies are present within them. Here we use CWT to localize the magnetic wave packets in rotationally adjusted northern (or southern) magnetic phase and frequency space. The units for phase used are "cycles since 1 January 2004" [*Yates et al.*, 2015].

The quasiperiodic nature of these wave packets is evident in Figure 2. Figures 2a and 2b show wavelet power in northern Andrews and Provan (AP) phase and inverse frequency (period) space for the $\delta b_{\perp\nu}$ and $\delta b_{\perp\phi}$ MFA magnetic field components, respectively. A "Morlet" wavelet—a plane wave modulated by a Gaussian envelope—is used to carry out the CWT. The maxima in Figures 2a and 2b represent the location of each wave packet in the northern phase and period space. The maxima typically lie between periods enclosed by the horizontal solid white lines corresponding to periods between 30 and 90 min. This implies that the magnetic fluctuations within each wave packet have a high probability of having periods between 30 and 90 min—comparable to the QP60 observations mentioned above.

The white vertical dashed lines in Figures 2a and 2b show integer values of northern phase [*Yates et al.*, 2015]. The wavelet maxima occur near integer values of northern phase suggesting a periodic recurrence of the wave packets. CWT was also performed using AP's southern phase producing maxima midway between integer values of southern phase. During this interval, AP's northern and southern magnetic phases were approximately in antiphase with each other; therefore, the difference of a half cycle between using northern or southern phase is expected and not shown. The analysis above suggests that the ∼1 h magnetic fluctuations are somehow modulated by the ∼10.7 h magnetic oscillations resulting in the observed wave packets. We investigate the wave packets periodic modulation/recurrence by performing Lomb-Scargle (LS) periodogram analysis on the wavelet powers for all three MFA magnetic components. LS is used in order to allow for gaps in the data, and it assumes phase continuity across the gaps. Each maximum in the wavelet power corresponds to the location of a separate wave packet. LS analysis on the wavelet maxima therefore establishes a recurrence frequency for the wave packets. Figure 2c presents LS results for our 6 day interval as a function of time, indicating enhanced power near the mean northern and southern magnetic oscillation periods (vertical dashed black lines at 634 and 649 min, respectively), but we are unable to differentiate between the two. We also carry out an LS analysis on a longer (∼150 day) interval spanning September 2006 through February 2007 using data only from the Northern Hemisphere (planetary latitude >15° and L>15 R_S) and using northern AP phase as input to the LS periodogram instead of time. Note that for this longer interval CWT edge effects are not included in the LS analysis. The results (Figure 2d) clearly show that the significant peaks occur at the northern oscillation frequency/phase (vertical solid black line), confirming that the wave packets at high northern latitudes are indeed modulated by, or recur at, the northern magnetic oscillation. There is some power associated with peaks at periods slightly longer than the southern magnetic period (range enclosed by vertical dashed black lines). We find that these result from the beating between the northern signal and the periodic data gaps arising from the repetitive spacecraft orbits (12, 16, and 18 days). These beat ranges are highlighted in Figure 2d.

4. Interpretation of Results: Structure and Origin of QP60 Pulsations

Many properties of the magnetic field and the plasma in Saturn's magnetosphere fluctuate with periods near 1 h. It seems improbable that the ∼1 h period is imposed by the solar wind, so we consider how it might arise as a natural frequency of the Kronian system. This observed period is comparable to estimates of the Alfvén wave travel time in Saturn's outer magnetosphere [*Bunce et al.*, 2005; *Roussos et al.*, 2016]. Moreover, *Meredith et al.* [2013] and *Carbary et al.* [2016] both propose that their observations are caused by interhemispheric Alfvén waves.

The transverse magnetic polarization of the QP60 magnetic fluctuations supports the assumption that the waves are Alfvénic. Recognizing that the plasma distribution along Kronian flux tubes is nonuniform, we next consider the form of Alfvén waves standing in a nonuniform background plasma distribution. We follow *Southwood and Kivelson* [1986] in using a magnetospheric box model with inhomogeneous plasma densities. Figure 3a shows a schematic of this model, with X representing radial distance. The magnetic field, B, is taken to be uniform, parallel to Z and bounded at $\pm \mathcal{L} R_S$ by highly conducting ionospheres. The plasma near the center of the box between $\pm z_o$ represents the equatorial magnetodisc and is assumed dense, with a low Alfvén speed. Elsewhere, the plasma density is low, as at high latitudes, and the Alfvén speed is high. We assume that the plasma density and the Alfvén speeds depend only on z, meaning that compressional and transverse waves are not coupled. One can then solve the wave equation

$$\left[v_A^2(z) \frac{\partial^2}{\partial z^2} + \omega_T^2 \right] \Omega_T(z) = 0, \tag{1}$$

where v_A is the Alfvén speed and ω_T is the eigenfrequency corresponding to the eigenfunction Ω_T. If Ω_T represents the plasma displacement wavefield and we assume that the plasma displacement is zero at the ionospheric boundaries, one can solve equation (1) for even and odd symmetry about $z = 0$. These analytical solutions can be found in *Southwood and Kivelson* [1986] and *Khurana and Kivelson* [1989], and the eigenfrequencies are solved numerically for even and odd symmetry respectively using [*Southwood and Kivelson*, 1986]:

$$v_{A_0}^{-1} \tan\left(\omega_T z_0 / v_{A_0} \right) = v_{A_1}^{-1} \cot\left[\omega_T (l - z_0) / v_{A_1} \right], \tag{2}$$
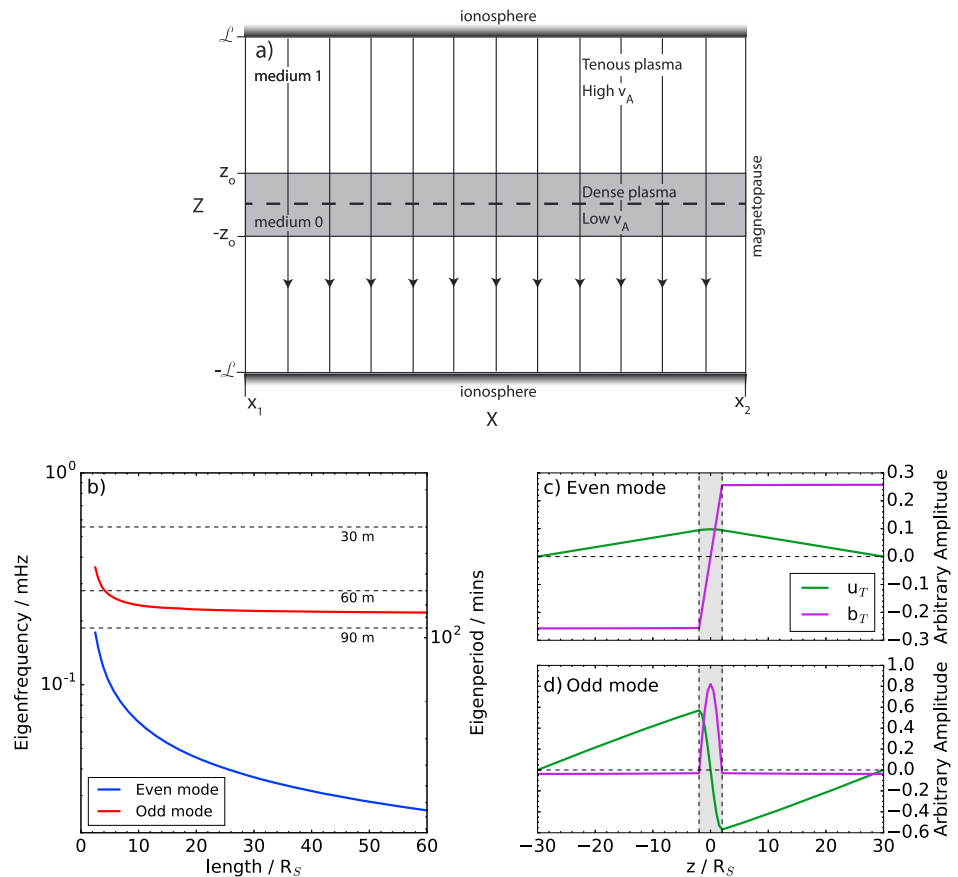
Figure 3. (a) Schematic of the inhomogeneous magnetospheric box model. Z represents the length of the magnetic field lines (solid black lines with arrows), and X represents equatorial radial distance. Medium 0 represents Saturn's plasma sheet, and medium 1 represents the high-latitude closed magnetosphere at Saturn. This has been adapted from *Southwood and Kivelson* [1986] and *Khurana and Kivelson* [1989]. (b) The corresponding eigenfrequencies of the first two harmonics (first/fundamental in blue and second in red) as a function of field line length [*Southwood and Kivelson*, 1986; *Khurana and Kivelson*, 1989]. The y axis on the right then shows the equivalent eigenperiods along with dashed lines highlighting our periods of interest (30, 60, and 90 min). (c) The plasma displacement (green line) and the magnetic field perturbation (purple line) caused by the fundamental wave for an $\mathcal{L}=30\ R_S$ field line with $z_o=2\ R_S$. The dense equatorial plasma sheet is shaded. (d) The same as Figure 3c but for the second harmonic wave.

$$v_{A_0}^{-1} \cot\left(\omega_T z_0/v_{A_0}\right) = -v_{A_1}^{-1} \cot\left[\omega_T(l-z_0)/v_{A_1}\right], \tag{3}$$

where l is the length of the field line. *Southwood and Kivelson* [1986] and *Khurana and Kivelson* [1989] show that if the Alfvén travel time is much larger in "medium 0" than in "medium 1," which is almost always valid in the Kronian/Jovian system, the approximate solutions to equation (1) tend to a state where they are independent of the Alfvén velocity in medium 1. Figure 3b shows how the eigenfrequency of a transverse wave changes with field line length for the even (fundamental) solution (blue) and for the odd (second harmonic) solution (red). For this analysis, we have taken $z_0 = 2\ R_S$, $v_{A_1} = 3500$ km s^{-1} (calculated from LP measurements), and $v_{A_0} = 105$ km s^{-1} (estimated from plasma density ($\sim 1 \times 10^4$ m^{-3}) and field ~ 2 nT measurements of Saturn's equatorial magnetosphere presented in *Arridge et al.* [2011] and assuming water ions only). The fundamental harmonic's eigenfrequency continues to decrease with increasing field line length, quickly approaching timescales comparable to Saturn's rotation rate. Such modes are likely not to be observable. In contrast, the second harmonic's frequency is relatively fixed with much smaller changes over the same interval of field line length. The timescales are sensitive to the parameters z_0 and v_{A_0} but remain comparable to the period of magnetic fluctuations presented above for reasonable values. For example, the second harmonic period ranges from 74 to 180 min with z_0 from 2 to 5 R_S [*Provan et al.*, 2012] and v_{A_0} as above. While the period ranges from 26 to 62 min with z_0 from 2 to 5 R_S, if we assume that the plasma sheet has only H$^+$ ions giving $v_{A_0} = 305$ km s^{-1}.
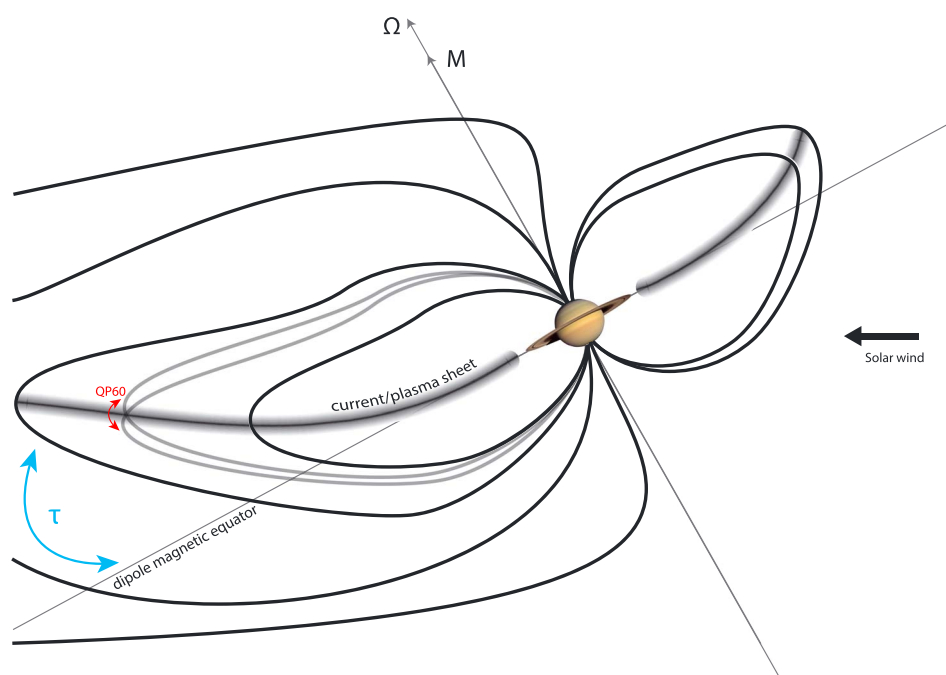
Figure 4. Schematic of Saturn's magnetosphere showing our physical interpretation. The black lines represent magnetic field lines, and the shaded central region represents the plasma sheet. The thick gray solid lines represent our interpretation of the maximum and minimum excursions of magnetic field lines perturbed by the second harmonic Alfvén waves. τ indicates the modulating period of the wave packets. In the case presented herein the modulating period is the northern magnetic oscillation.

Figures 3c and 3d show how the plasma displacement (green lines) and transverse magnetic field perturbation (purple lines) vary with z for even and odd modes, respectively. The boundary conditions require plasma displacement nodes at the ionospheric boundaries for both modes. The even mode magnetic perturbations have antinodes at the nominal ionospheric boundaries and a node at the magnetic equator. This implies that the fluctuations should have largest amplitudes at high latitudes. The odd mode magnetic perturbation amplitude is largest within the plasma sheet near the equator and is small off the equator. These characteristics are consistent with our observations. *Khurana and Kivelson* [1989] inferred similar structure for low-frequency waves at Jupiter.

The form of these transverse fluctuations along with their eigenfrequencies lead us to propose that the magnetic fluctuations shown in Figures 1g and 1h are second (odd) harmonic Alfvén waves on closed outer magnetospheric field lines. The dense equatorial plasma sheet reduces the amplitude of the fluctuations in the low-density high-latitude region which we observe. The varying density of the equatorial plasma sheet [*Provan et al.*, 2012] also explains why the wave period observed is not fixed at ~1 h but varies by ~20%.

The wave packet structure of the QP60 waves also requires interpretation. We propose that the wave packet structure is imposed by "rocking" of the magnetosphere with respect to the spacecraft, with a modulation of intensity resulting from the ~10.7 h variations of magnetospheric configuration. The modulation would be dominated by the northern period at high northern latitudes and by the southern period at high southern latitudes [*Provan et al.*, 2012]. Rocking of flux tubes changes the relative position of the spacecraft with respect to the high-density equatorial region resulting in an increase or decrease in the amplitude of the magnetic fluctuations. The Alfvénic nature of the waves, combined with the fact that the Alfvén mode carries field-aligned currents [*Southwood and Hughes*, 1983], leads us to associate these waves with magnetosphere-ionosphere coupling. A schematic of our interpretation applicable to the 2006 era is shown in Figure 4. Here Saturn and its magnetosphere are shown with the thick black lines representing magnetic field lines and the shaded region representing the equatorial plasma sheet. The two thick gray lines illustrate the maximum and minimum perturbed second harmonic plasma displacement states with nodes at the center of the plasma sheet and polar ionospheres.

5. Conclusion

We have presented observations of transverse quasiperiodic magnetic field fluctuations possessing periods of ∼60 m and found an explanation as to their nature. Our work showed that these fluctuations are Alfvénic and that the wave packets containing them recur periodically, following the northern magnetic oscillation phase in the northern magnetosphere. In addition, the associated density variations suggest that the wave packet structure is created by the rocking of the magnetosphere. Using a magnetospheric box model with a nonuniform distribution of density along flux tubes that represents the concentration of plasma density near Saturn's magnetic equator, we demonstrated that the observed magnetic fluctuations represent second harmonic Alfvénic perturbations standing between the northern and southern ionospheres in Saturn's outer magnetosphere. Such waves should be fairly well confined to outer magnetospheric field lines due to the large change in Alfvén speed within the more dense middle/inner magnetosphere. These Alfvén waves should be associated with magnetosphere-ionosphere coupling processes. They are also the MHD mode that carries field-aligned currents and so would be involved in creating the pulsating signatures observed in previous studies (see review by *Keiling* [2009] for the terrestrial system). Our model assumptions do not provide insight into the generation mechanism for these Alfvén waves, but they are probably generated by some dynamical process occurring in the outer magnetosphere or in the central plasma sheet. *Meredith et al.* [2013] also suggested that field-aligned currents of second harmonic Alfvén resonances were responsible for their observations of conjugate auroral patches at Saturn. A future study relevant to the present work will use a larger data set over the entire Cassini mission thus far in order to further investigate these Alfvén waves in all magnetospheric regions, their spectral structure, and their relation to the other quasiperiodic phenomena discussed above.

References

Achilleos, N., P. Guio, and C. S. Arridge (2010), A model of force balance in Saturn's magnetodisc, *Mon. Not. R. Astron. Soc.*, *401*, 2349–2371, doi:10.1111/j.1365-2966.2009.15865.x.

Andrews, D. J., et al. (2010), Magnetospheric period oscillations at Saturn: Comparison of equatorial and high-latitude magnetic field periods with north and south Saturn kilometric radiation periods, *J. Geophys. Res.*, *115*, A12252, doi:10.1029/2010JA015666.

Andrews, D. J., et al. (2012), Planetary period oscillations in Saturn's magnetosphere: Evolution of magnetic oscillation properties from southern summer to post-equinox, *J. Geophys. Res.*, *117*, A04224, doi:10.1029/2011JA017444.

Arridge, C. S., et al. (2008), Warping of Saturn's magnetospheric and magnetotail current sheets, *J. Geophys. Res.*, *113*, A08217, doi:10.1029/2007JA012963.

Arridge, C. S., et al. (2011), Periodic motion of Saturn's nightside plasma sheet, *J. Geophys. Res.*, *116*, A11205, doi:10.1029/2011JA016827.

Badman, S. V., et al. (2012), Cassini observations of ion and electron beams at Saturn and their relationship to infrared auroral arcs, *J. Geophys. Res.*, *117*, A01211, doi:10.1029/2011JA017222.

Badman, S. V., et al. (2016), Saturn's auroral morphology and field-aligned currents during a solar wind compression, *Icarus*, *263*, 83–93, doi:10.1016/j.icarus.2014.11.014.

Bagenal, F., et al. (2014), Magnetospheric science objectives of the Juno mission, *Space. Sci. Rev.*, 1–69, doi:10.1007/s11214-014-0036-8.

Brown, R. H., et al. (2004), The Cassini visual and infrared mapping spectrometer (VIMS) investigation, *Space Sci. Rev.*, *115*, 111–168, doi:10.1007/s11214-004-1453-x.

Bunce, E. J., S. W. H. Cowley, and S. E. Milan (2005), Interplanetary magnetic field control of Saturn's polar cusp aurora, *Ann. Geophys.*, *23*, 1405–1431, doi:10.5194/angeo-23-1405-2005.

Bunce, E. J., et al. (2014), Cassini nightside observations of the oscillatory motion of Saturn's northern auroral oval, *J. Geophys. Res.*, *119*, 3528–3543, doi:10.1002/2013JA019527.

Carbary, J. F., W. S. Kurth, and D. G. Mitchell (2016), Short periodicities in low-frequency plasma waves at Saturn, *J. Geophys. Res. Space Physics*, *121*, 6562–6572, doi:10.1002/2016JA022732.

Carlson, C. W., et al. (1998), FAST observations in the downward auroral current region: Energetic upgoing electron beams, parallel potential drops, and ion heating, *Geophys. Res. Lett.*, *25*, 2017–2020, doi:10.1029/98GL00851.

Chen, L., and A. Hasegawa (1974), A theory of long-period magnetic pulsations: 1. Steady state excitation of field line resonance, *J. Geophys. Res.*, *79*, 1024–1032, doi:10.1029/JA079i007p01024.

Cramm, R., K.-H. Glassmeier, M. Stellmacher, and C. Othmer (1998), Evidence for resonant mode coupling in Saturn's magnetosphere, *J. Geophys. Res.*, *103*, 11,951–11,960, doi:10.1029/98JA00629.

Delamere, P. A. (2016), A review of the low-frequency waves in the giant magnetospheres, in *Low-Frequency Waves in Space Plasmas*, vol. 216, pp. 365–378, Wiley, Hoboken, N. J., doi:10.1002/9781119055006.ch21.

Dougherty, M. K., et al. (2004), The Cassini magnetic field investigation, *Space Sci. Rev.*, *114*, 331–383, doi:10.1007/s11214-004-1432-2.

Dougherty, M. K., et al. (2005), Cassini magnetometer observations during Saturn orbit insertion, *Science*, *307*, 1266–1270, doi:10.1126/science.1106098.

Dungey, J. W. (1955), Electrodynamics of the outer atmosphere, in *Physics of the Ionosphere*, p. 229, The Physical Society, London.

Galopeau, P. H. M., and A. Lecacheux (2000), Variations of Saturn's radio rotation period measured at kilometer wavelengths, *J. Geophys. Res.*, *105*, 13,089–13,102, doi:10.1029/1999JA005089.

Glassmeier, K.-H., F. M. Neubauer, N. F. Ness, and M. H. Acuna (1989), Standing hydromagnetic waves in the Io plasma torus—Voyager 1 observations, *J. Geophys. Res.*, *94*, 15,063–15,076, doi:10.1029/JA094iA11p15063.

Glassmeier, K.-H., D. Klimushkin, C. Othmer, and P. Mager (2004), ULF waves at Mercury: Earth, the giants, and their little brother compared, *Adv. Space Res.*, *33*, 1875–1883, doi:10.1016/j.asr.2003.04.047.

Gurnett, D. A., et al. (2004), The Cassini radio and plasma wave investigation, *Space Sci. Rev.*, *114*, 395–463, doi:10.1007/s11214-004-1434-0.

Gurnett, D. A., et al. (2009), Discovery of a north-south asymmetry in Saturn's radio rotation period, *Geophys. Res. Lett.*, *36*, L16102, doi:10.1029/2009GL039621.

Gurnett, D. A., et al. (2010), A plasmapause-like density boundary at high latitudes in Saturn's magnetosphere, *Geophys. Res. Lett.*, *37*, L16806, doi:10.1029/2010GL044466.

Hunt, G. J., et al. (2014), Field-aligned currents in Saturn's southern nightside magnetosphere: Subcorotation and planetary period oscillation components, *J. Geophys. Res. Space Physics*, *119*, 9847–9899, doi:10.1002/2014JA020506.

Kanani, S. J., et al. (2010), A new form of Saturn's magnetopause using a dynamic pressure balance model, based on in situ, multi-instrument Cassini measurements, *J. Geophys. Res.*, *115*, A06207, doi:10.1029/2009JA014262.

Keiling, A. (2009), Alfvén waves and their roles in the dynamics of the Earth's magnetotail: A review, *Space Sci. Rev.*, *142*, 73–156, doi:10.1007/s11214-008-9463-8.

Khurana, K. K., and M. G. Kivelson (1989), Ultralow frequency MHD waves in Jupiter's middle magnetosphere, *J. Geophys. Res.*, *94*, 5241–5254, doi:10.1029/JA094iA05p05241.

Kivelson, M. G., and D. J. Southwood (1985), Resonant ULF waves—A new interpretation, *Geophys. Res. Lett.*, *12*, 49–52, doi:10.1029/GL012i001p00049.

Kleindienst, G., K.-H. Glassmeier, S. Simon, M. K. Dougherty, and N. Krupp (2009), Quasiperiodic ULF—Pulsations in Saturn's magnetosphere, *Ann. Geophys.*, *27*, 885–894, doi:10.5194/angeo-27-885-2009.

Krimigis, S. M., et al. (2004), Magnetosphere Imaging Instrument (MIMI) on the Cassini mission to Saturn/Titan, *Space Sci. Rev.*, *114*, 233–329, doi:10.1007/s11214-004-1410-8.

Kurth, W. S., A. Lecacheux, T. F. Averkamp, J. B. Groene, and D. A. Gurnett (2007), A Saturnian longitude system based on a variable kilometric radiation period, *Geophys. Res. Lett.*, *34*, L02201, doi:10.1029/2006GL028336.

Meredith, C. J., S. W. H. Cowley, K. C. Hansen, J. D. Nichols, and T. K. Yeoman (2013), Simultaneous conjugate observations of small-scale structures in Saturn's dayside ultraviolet auroras: Implications for physical origins, *J. Geophys. Res. Space Physics*, *118*, 2244–2266, doi:10.1002/jgra.50270.

Mitchell, D. G., et al. (2009), Ion conics and electron beams associated with auroral processes on Saturn, *J. Geophys. Res.*, *114*, A02212, doi:10.1029/2008JA013621.

Mitchell, D. G., et al. (2016), Recurrent pulsations in Saturn's high latitude magnetosphere, *Icarus*, *263*, 94–100, doi:10.1016/j.icarus.2014.10.028.

Palmaerts, B., et al. (2016), Statistical analysis and multi-instrument overview of the quasi-periodic 1-hour pulsations in Saturn's outer magnetosphere, *Icarus*, *271*, 1–18, doi:10.1016/j.icarus.2016.01.025.

Provan, G., et al. (2012), Dual periodicities in planetary-period magnetic field oscillations in Saturn's tail, *J. Geophys. Res.*, *117*, A01209, doi:10.1029/2011JA017104.

Radioti, A., et al. (2011), Bifurcations of the main auroral ring at Saturn: Ionospheric signatures of consecutive reconnection events at the magnetopause, *J. Geophys. Res.*, *116*, A11209, doi:10.1029/2011JA016661.

Radioti, A., et al. (2013), Auroral signatures of multiple magnetopause reconnection at Saturn, *Geophys. Res. Lett.*, *40*, 4498–4502, doi:10.1002/grl.50889.

Roussos, E., et al. (2016), Quasi-periodic injections of relativistic electrons in Saturn's outer magnetosphere, *Icarus*, *263*, 101–116, doi:10.1016/j.icarus.2015.04.017.

Southwood, D. J. (1974), Some features of field line resonances in the magnetosphere, *Planet and Space Sci.*, *22*, 483–491, doi:10.1016/0032-0633(74)90078-6.

Southwood, D. J., and W. J. Hughes (1983), Theory of hydromagnetic waves in the magnetosphere, *Space Sci. Rev.*, *35*, 301–366, doi:10.1007/BF00169231.

Southwood, D. J., and M. G. Kivelson (1986), The effect of parallel inhomogeneity on magnetospheric hydromagnetic wave coupling, *J. Geophys. Res.*, *91*, 6871–6876, doi:10.1029/JA091iA06p06871.

Southwood, D. J., and M. G. Kivelson (2007), Saturnian magnetospheric dynamics: Elucidation of a camshaft model, *J. Geophys. Res.*, *112*, A12222, doi:10.1029/2007JA012254.

Takahashi, K., P. J. Chi, R. E. Denton, and R. L. Lysak (Eds.) (2006), *Magnetospheric ULF Waves: Synthesis and New Directions, Geophys. Monogr. Ser.*, vol. 169, doi:10.1029/GM169.

Warner, M. R., and D. Orr (1979), Time of flight calculations for high latitude geomagnetic pulsations, *Planet. Space Sci.*, *27*, 679–689, doi:10.1016/0032-0633(79)90165-X.

Yates, J. N., D. J. Southwood, and M. K. Dougherty (2015), Magnetic phase structure of Saturn's 10.7 h oscillations, *J. Geophys. Res.*, *120*, 2631–2648, doi:10.1002/2014JA020629.

Young, D. T., et al. (2004), Cassini plasma spectrometer investigation, *Space Sci. Rev.*, *114*, 1–112, doi:10.1007/s11214-004-1406-4.